Pergamon

Int. J. Solids Structures Vol. 31, No. 20, pp. 2753–2768, 1994
Elsevier Science Ltd
Printed in Great Britain
0020-7683/94 $7.00 + .00

0020-7683(94)E0055-Z

MULTIPLE CRACKING IN METAL–CERAMIC LAMINATES

Y. HUANG, H. W. ZHANG and F. WU
Department of Aerospace and Mechanical Engineering, The University of Arizona, Tucson, AZ 85721, U.S.A.

(*Received* 31 *March* 1993; *in revised form* 29 *March* 1994)

Abstract—There have been observations showing that relatively thick metal layers in metal–ceramic laminates lead to the formation of multiple periodic cracks within a zone near a pre-crack, distributing damage and significantly enhancing the composite's toughness. Several models including linear elastic fracture mechanics and shear-lag analysis are developed in the present work in order to study the competition between multiple cracking and single-crack extension as damage modes. It is established that there is a critical thickness ratio for metal–ceramic layers above which multiple cracking dominates. Moreover, this critical thickness ratio is inversely proportional to the corresponding moduli ratio such that the competition between damage modes is governed by the metal–ceramic layer stiffness ratio. Plastic hardening of metals helps to activate the multiple-cracking damage mode, while plastic yielding does the opposite.

1. INTRODUCTION

Metal–ceramic laminates are an important class of composite materials because they can be readily fabricated while controlling interfacial and constituent properties (e.g. Evans *et al.*, 1986; Dalgleish *et al.*, 1988). The mechanical properties of metals, ceramics, interfaces and other parameters, such as ceramic volume fraction in a laminate, can be chosen to maximize the desired mechanical properties of the laminate. The toughening of ceramic composites has always been a major concern with regard to their application; therefore, achieving the highest possible toughness of ceramic composites has been the aim of many researchers (e.g. Dalgleish *et al.*, 1989).

The toughness of metal–ceramic laminates originates in the plastic deformation of the metals. The microcracks in brittle ceramic layers generated by applied loading or residual stresses may be arrested by neighboring metal layers (Cao and Evans, 1991), which leads to plastic deformation in the metal layers. The crack tip stress concentration is significantly dissipated due to plastic flow, thus the toughness of the laminate can be increased.

Different damage modes in metal–ceramic laminates have been observed. Deve and Maloney (1991) and Deve *et al.* (1992) found that the formation of a zone of periodic cracks is one damage mode, and the extension of a (single) dominant crack is another. They established that the former mode distributes the damage and significantly enhances the composite's toughness. The aim of the present paper is to study conditions that will facilitate this multiple-cracking damage mode.

A simple criterion separating these two damage modes based on the perspective of maximum stress in ceramic layers is developed in Section 2. This criterion is carried out in the following sections by different methods, including linear elastic fracture mechanics and the shear-lag method, in order to study the effect of metal–ceramic layer thickness ratio, moduli, and plastic yielding and hardening on the competition between the multiple-cracking mode and the dominant crack extension mode.

2. MULTIPLE CRACKING VERSUS SINGLE-CRACK EXTENSION

Shaw *et al.* (1993) studied the nucleation of a microcrack in ceramics across a metal layer in metal–ceramic laminates. Ceramics are brittle and vulnerable to microcracking, while the plastic flow in metals dissipates the stress concentration in metal layers in order

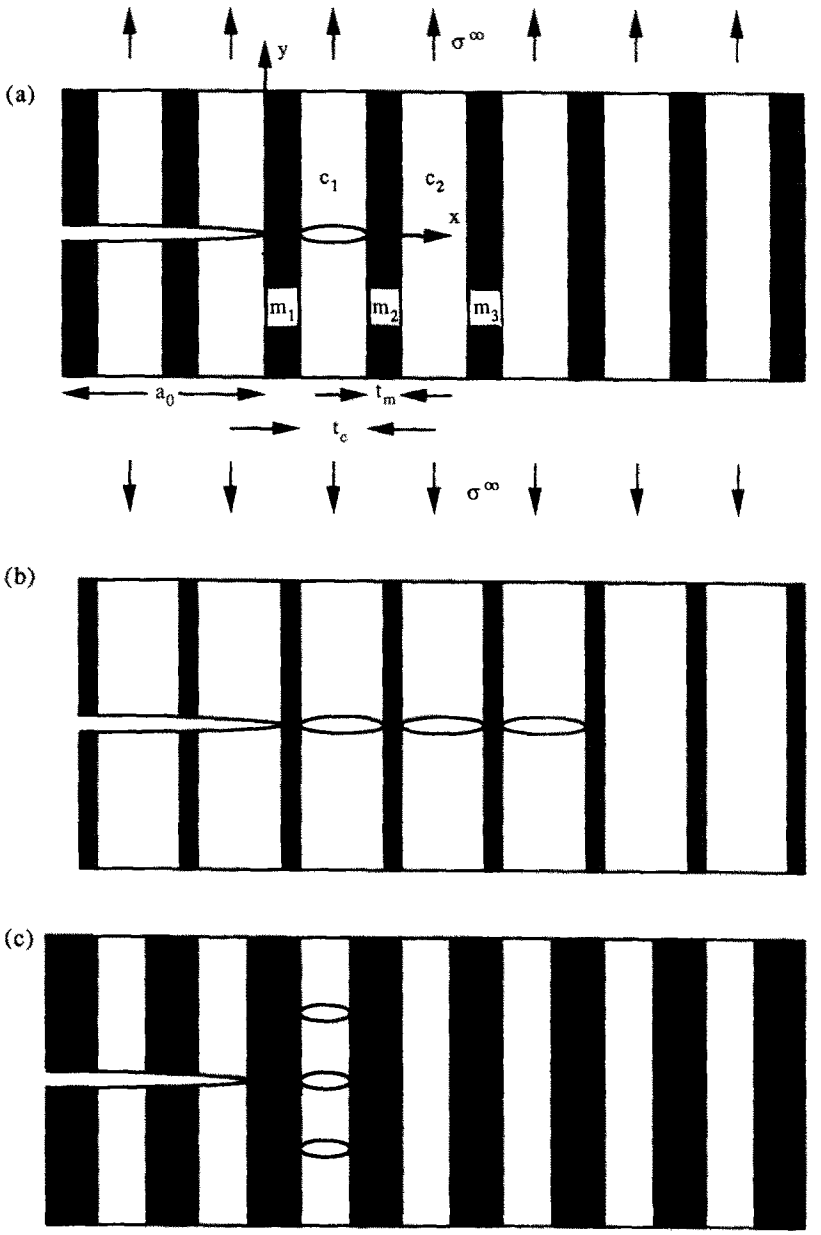

Fig. 1. A configuration of metal–ceramic laminates: (a) crack renucleation in a ceramic layer; (b) single-crack extension in ceramic layers after crack renucleation; (c) multiple cracking ceramic layers after crack renucleation.

to avoid microstructure damage and to provide the toughness of a composite. As shown in Fig. 1(a), a pre-existing edge crack in metal–ceramic laminates results in stress concentration ahead of the crack tip, thereby nucleating a microcrack along the crack plane in the next ceramic layer [layer c_i in Fig. 1(a)]. This so-called crack renucleation phenomenon has been studied by Dalgleish *et al.* (1989) and Cao and Evans (1991). The renucleated crack penetrates the ceramic layer and is arrested by two neighboring metal layers. After crack renucleation, if metal layers remain intact [as shown in Fig. 1(a) by darkened metal segments in the crack plane], multiple cracking or a single-crack extension may occur. Shaw *et al.* (1993) pointed out that, subsequent to crack renucleation, relatively thick ceramic layers lead to damage in the form of continuous microcracking in the adjacent ceramic layers along the plane of the pre-existing edge crack [Fig. 1(b)] and that thin ceramic layers cause the formation of multiple periodic cracks within a zone near the pre-crack [Fig. 1(c)]. This formation of a multiple-cracking zone distributes damage and significantly enhances the

composite toughness as compared to the extension of a dominant crack (Deve and Maloney, 1991; Deve *et al.*, 1992).

The objective of this paper is to quantitatively determine the critical thickness of ceramic layers below which multiple cracking prevails over single-crack extension in metal–ceramic laminates. A configuration of metal–ceramic laminates after crack renucleation [Fig. 1(a)] is used in the present study. In this configuration, the maximum stress in the ceramic layer in which a microcrack has been renucleated [layer c_1 in Fig. 1(a)] occurs somewhere above the crack plane. This maximum stress, σ_{max}, is compared to σ_0, the stress on the crack plane in the next (*unbroken*) ceramic layer [layer c_2 in Fig. 1(a)]. If σ_{max} is larger than σ_0, the next microcrack will be nucleated at the site of σ_{max}, i.e. somewhere above the renucleated crack in the same ceramic layer (layer c_1). Therefore, multiple cracking will dominate when $\sigma_{max} > \sigma_0$. If σ_{max} is less than σ_0, the next microcrack will be nucleated in the next (unbroken) ceramic layer (layer c_2) along the crack plane such that single-crack extension prevails.

It is evident that this critical thickness of ceramic layers, or the critical thickness ratio of metal–ceramic layers, which distinguishes multiple cracking from a single-crack extension, depends on elastic properties of the metal and ceramic, the plastic yielding and hardening of the metal, and the pre-crack length. Different models to examine the competition between multiple cracking and single-crack extension in metal–ceramic laminates are proposed in the following sections: a fracture mechanics analysis is presented in Section 3, and several shear-lag models are presented in Section 4. For simplicity, the analysis is limited to two dimensions, i.e. plane-strain analysis.

3. LINEAR ELASTIC FRACTURE MECHANICS ANALYSIS

We begin the examination of the critical metal—ceramic thickness ratio by considering the simplest laminates—metal and ceramic layers are elastic with the same elastic properties. (The effects of metal plasticity and the metal–ceramic moduli ratio are examined in following sections.) Thus, the laminate can be considered as a uniform medium. As shown in Fig. 1(a), there is a pre-existing edge crack of length a_0 starting from the left edge of the metal–ceramic laminate. The thicknesses of the metal and ceramic layers are t_m and t_c, respectively. The laminate is subject to remote tension, σ^∞, in the laminate direction. A microcrack has been renucleated in the next ceramic layer (layer c_1) along the pre-crack plane, while the metal layer between the two cracks remains intact. For simplicity, it is assumed that there are many unbroken layers to the right of the renucleated crack, so the effect of the right boundary of the laminate is neglected.

The stress distribution in the metal–ceramic laminate can be analysed using linear elastic fracture mechanics (LEFM). The pre-crack and the renucleated crack are modeled as two continuously distributed dislocations (Rice, 1968), which leads to two integral equations governing dislocation densities for two cracks. These integral equations, given in the Appendix, are solved numerically along the lines proposed by Erdogan *et al.* (1973). The stress variation over thickness direction in each ceramic layer is small because ceramic layers are thin compared to the pre-crack length, i.e. $t_c \ll a_0$; therefore, the stress in ceramic layers is well approximated by the average stress over the thickness. The average stress in the ceramic layer that contains the renucleated crack [layer c_1 in Fig. 1(a)] is

$$\bar{\sigma}_1(y) = \frac{1}{t_c}\int_{t_m}^{t_m+t_c} \sigma_{yy}(x, y)\,dx, \tag{1}$$

where the origin of the coordinate (x, y) coincides with the pre-crack tip, and the x-axis is normal to the laminate direction. The average stress in the next (unbroken) ceramic layer [layer c_2 in Fig. 1(a)] is

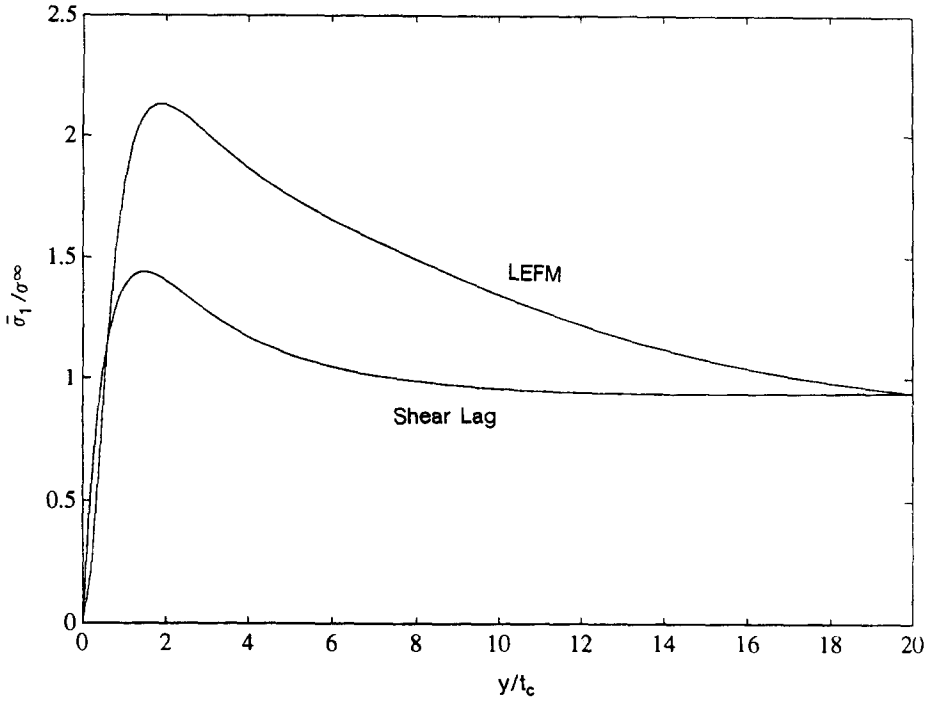

Fig. 2. Axial stress distribution in the ceramic layer that contains the renucleated crack, where $E_m = E_c$, $t_m = t_c$, $\nu = 0.3$ and $a_0 = 5(t_m + t_c)$.

$$\bar{\sigma}_2(y) = \frac{1}{t_c}\int_{2t_m+t_c}^{2t_m+2t_c} \sigma_{yy}(x, y)\,dx. \tag{2}$$

The maximum stress in the ceramic layer that contains the renucleated crack, σ_{max}, and the stress at the crack plane in the next (unbroken) ceramic layer, σ_0, are of particular interest. They are given by

$$\sigma_{max} = \max_y \{\bar{\sigma}_1(y)\} \quad \text{and} \quad \sigma_0 = \bar{\sigma}_2(y = 0), \tag{3}$$

respectively. The maximum stress, σ_{max}, occurs somewhere above the crack plane, as shown in Fig. 2, in which $\bar{\sigma}_1(y)/\sigma^\infty$ is plotted versus y/t_c for $t_m = t_c$, $\nu = 0.3$, and $a_0 = 5(t_m + t_c)$.

From a dimensional analysis, σ_{max} and σ_0 must have the form

$$\sigma_{max} = \sigma^\infty \cdot \Sigma^I_{max}\left(\frac{t_m}{t_c}, \frac{a_0}{t_m + t_c}, \nu\right) \tag{4}$$

$$\sigma_0 = \sigma^\infty \cdot \Sigma^I_0\left(\frac{t_m}{t_c}, \frac{a_0}{t_m + t_c}, \nu\right), \tag{5}$$

where σ^∞ is the applied stress, and Σ^I_{max} and Σ^I_0 are nondimensional functions depending on the metal–ceramic layer thickness ratio, pre-crack length and Poisson's ratio, ν (ν is the same for metals and ceramics, as assumed). The normalized pre-crack length, $a_0/(t_m + t_c)$, gives the number of pairs of metal–ceramic layers that are cut before the load is applied to the laminate. For thin metal layers, the effect of the renucleated crack is easily transmitted to the next (unbroken) ceramic layer [layer c_2 in Fig. 1(a)], so σ_0 is larger than σ_{max}. For thick metal layers, the opposite occurs (i.e. $\sigma_0 < \sigma_{max}$) because the next (unbroken) ceramic layer is relatively far from both cracks. Therefore, there exists a critical metal–ceramic layer thickness ratio, $(t_m/t_c)_{crit}$, at which $\sigma_{max} = \sigma_0$. From eqns (4) and (5), this critical thickness ratio must have the form

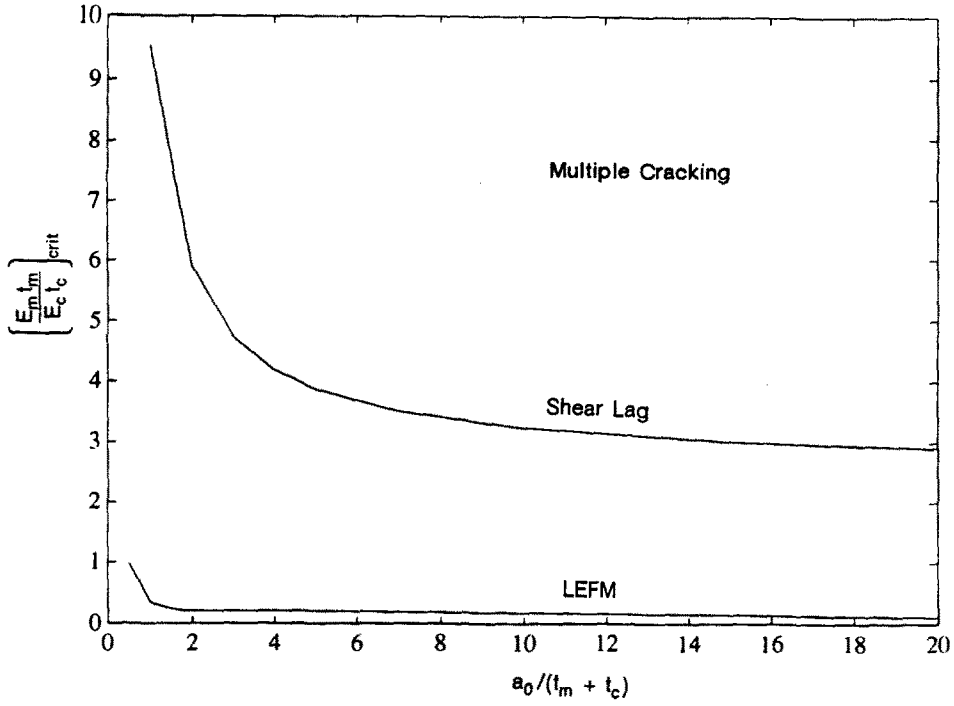

Fig. 3. Critical metal–ceramic layer stiffness ratio, $(E_m t_m/E_c t_c)$, which separates the multiple-cracking damage mode from single-crack extension, versus pre-crack length, $a_0/(t_m+t_c)$.

$$\left(\frac{t_m}{t_c}\right)_{crit} = f_{LEFM}\left(\frac{a_0}{t_m+t_c}, \nu\right). \tag{6}$$

The nondimensional function, f_{LEFM}, versus the pre-crack length, $a_0/(t_m+t_c)$, is shown in Fig. 3 for Poisson's ratio $\nu = 0.3$. This curve separates the regions of multiple cracking and single-crack extension. For a pre-cracked metal–ceramic laminate, if the thickness ratio t_m/t_c falls below the curve, σ_0 is larger than σ_{max} such that single-crack extension prevails. Multiple cracking will dominate if the thickness ratio is above the curve because $\sigma_{max} > \sigma_0$. The curve in Fig. 3 is very flat for $a_0 > 2(t_m+t_c)$, which shows that the competition between multiple cracking and single-crack extension is roughly independent of the pre-crack length, except for very short pre-cracks. It must be emphasized that the effects of metal plasticity and the metal–ceramic moduli ratio are not included in the LEFM model.

4. SHEAR-LAG ANALYSIS

Shear-lag analysis has been successfully applied to metal–ceramic laminates (e.g. Cao and Evans, 1991) and fiber-reinforced metal matrix composites (e.g. Budiansky *et al.*, 1986). In a shear-lag analysis, the stress, σ_n, in the laminate direction in each layer is averaged over the thickness. The laminate is subjected to remote applied stress, σ_∞. There are shear tractions in each layer at the interfaces with neighboring metal or ceramic layers. A shear-lag analysis greatly simplifies the problem without losing its characteristic features. The axial stress distribution, $\sigma_n(y)$, is the average stress over the layer thickness and is independent of x, where n is the layer number. For a metal–ceramic laminate, a shear-lag analysis leads to a set of ordinary differential equations of $\sigma_n(y)$ (see the Appendix for details). Only the upper half of the laminate ($y > 0$) is analysed due to symmetry. The boundary conditions are

$$\sigma_n = 0 \quad \text{at } y = 0 \tag{7a}$$

on the surface of the pre-crack and renucleated crack, and

$$w_n = 0 \quad \text{at } y = 0 \tag{7b}$$

for metal and ceramic layers that remain intact, where w_n is the displacement in the nth layer. A uniform applied strain, ε^∞, is imposed on the laminate to prevent sliding between metal and ceramic layers in the remote field. The corresponding applied stress imposed on the composite is

$$\sigma^\infty = [f\bar{E}_c + (1-f)\bar{E}_m]\varepsilon^\infty, \tag{8}$$

where f is the volume concentration of the ceramic and is related to the thickness of the metal–ceramic layer by $f = t_c/(t_m + t_c)$; $\bar{E}_c = E_c/(1-\nu_c^2)$ and $\bar{E}_m = E_m/(1-\nu_m^2)$ are the plane-strain elastic moduli for ceramic and metals, respectively.

4.1. *Elastic model*

A shear-lag analysis is particularly convenient for layered material with different elastic properties and with plastic deformation. Though the method is readily applied to metal layers that undergo plastic deformation, the analysis in this section is limited to elastic deformations only. The governing equation becomes a set of *linear* ordinary differential equations. The shear-lag stress distribution in the ceramic layer that contains the renucleated crack [layer c_1 in Fig. 1(a)] is compared with the LEFM model in Fig. 2, where the modeling parameters are $E_m = E_c$, $t_m = t_c$ and $a_0 = 5(t_m + t_c)$; E_m and E_c are the elastic moduli of the metal and ceramic, respectively. The elastic model indeed captures the feature that maximum stress occurs somewhere above the crack plane, although the peak stress is less than that estimated by the LEFM model. It is also observed that the positions of maximum stress, y/t_c, predicted by these two models agree well.

For a metal–ceramic laminate with different elastic properties, the maximum stress in the ceramic layer containing a renucleated crack, σ_{max}, and the stress at $y = 0$ in the next (unbroken) ceramic, σ_0, must have the following form from a dimensional analysis:

$$\sigma_{max} = \sigma^\infty \Sigma^{II}_{max}\left(\frac{t_m}{t_c}, \frac{a_0}{t_m + t_c}, \frac{E_m}{E_c}, \nu_m, \nu_c\right) \tag{9}$$

$$\sigma_0 = \sigma^\infty \Sigma^{II}_{0}\left(\frac{t_m}{t_c}, \frac{a_0}{t_m + t_c}, \frac{E_m}{E_c}, \nu_m, \nu_c\right), \tag{10}$$

where Σs are nondimensional functions.

The stresses, σ_{max} and σ_0, for a metal–ceramic laminate with the same elastic moduli, $E_m = E_c$, are plotted versus the metal–ceramic layer thickness ratio, t_m/t_c, in Fig. 4, where $a_0 = 5(t_m + t_c)$. As the ratio t_m/t_c increases, σ_{max} exceeds σ_0 and multiple cracking dominates. This has also been observed in the LEFM model. Therefore, for each moduli ratio, E_m/E_c, and pre-crack length, a_0, there exists a critical metal–ceramic layer thickness ratio above which σ_{max} is larger than σ_0 so that multiple cracking occurs. This relation between the critical thickness ratio, $(t_m/t_c)_{crit}$ (as determined by $\sigma_{max} = \sigma_0$), and the ceramic–metal moduli ratio, E_c/E_m, is presented in Fig. 5 for short, medium and long pre-cracks, $a_0/(t_m + t_c) = 1$, 5 and 20, respectively. It is observed from Fig. 5 that a linear relation between $(t_m/t_c)_{crit}$ and E_c/E_m always holds. This linear relationship is not trivial because a nondimensional analysis of the shear-lag model (given in the Appendix) shows that, in general, the stresses in metal and ceramic layers depend on two combinations of metal–ceramic layer properties, $E_m t_m/E_c t_c$ and $E_m t_c/E_c t_m$. From the numerical solution of the ordinary differential equations for the shear-lag model, it is found that the dependence on the second combination,

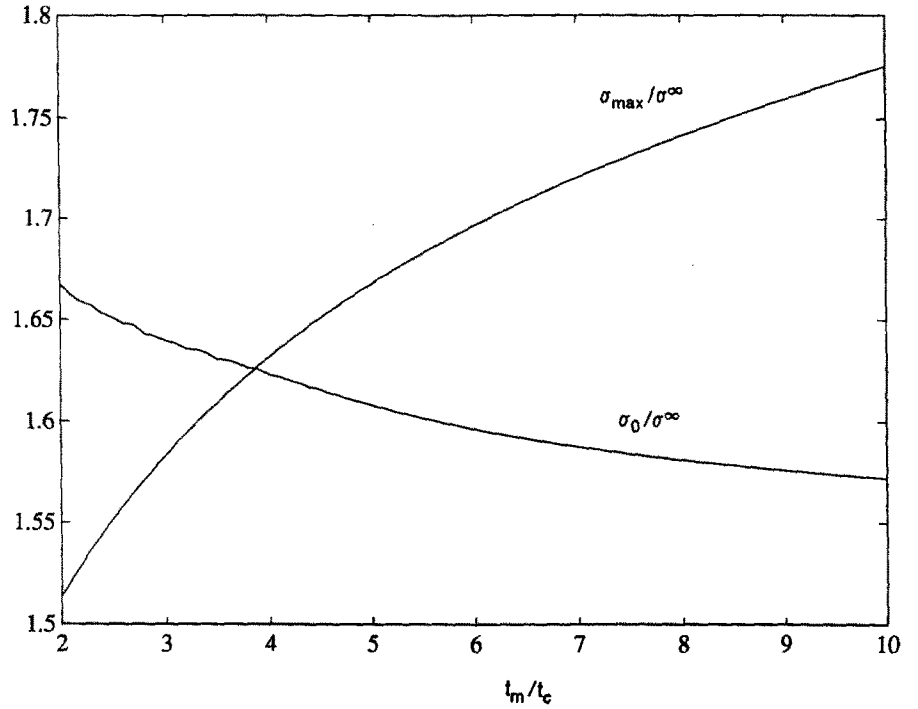

Fig. 4. Maximum stress, σ_{max}, in the ceramic layer that contains the renucleated crack and stress, σ_0, at the crack plane in the next (unbroken) ceramic layer versus the metal–ceramic layer thickness ratio, where $E_m = E_c$ and $a_0 = 5(t_m + t_c)$.

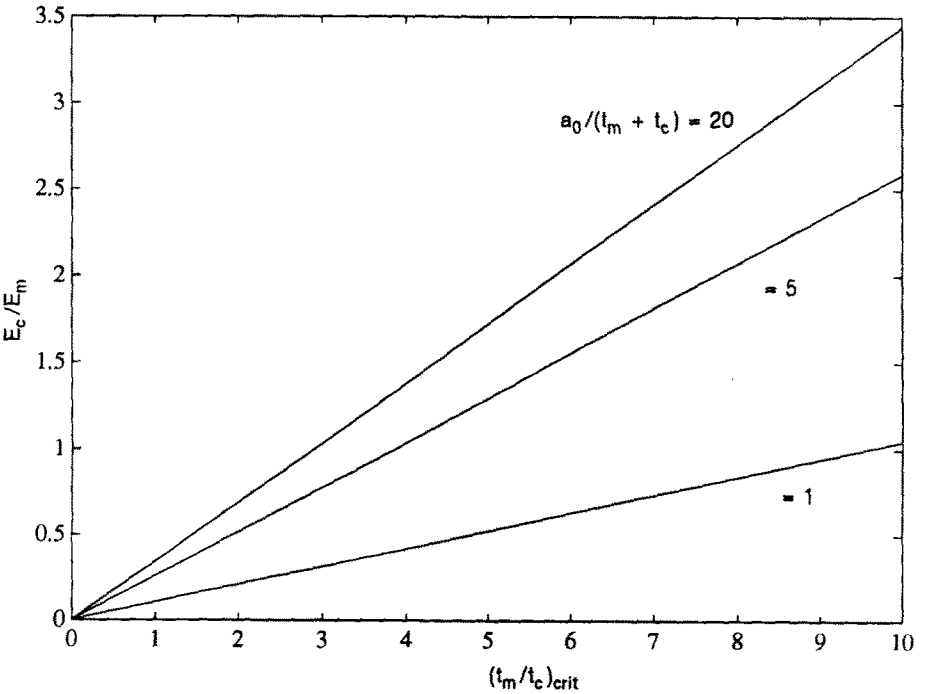

Fig. 5. The linear relation between critical metal–ceramic layer thickness ratio, $(t_m/t_c)_{crit}$, and ceramic–metal modulus ratio, E_c/E_m, for $a_0/(t_m + t_c) = 1$, 5 and 20.

$E_m t_c/E_c t_m$, is extremely weak. The linear relationship between $(t_m/t_c)_{crit}$ and E_c/E_m is established from $\sigma_{max} = \sigma_0$ and their sole dependence on the first combination, $E_m t_m/E_c t_c$. Therefore, the competition between multiple cracking and single-crack extension is determined by their layer stiffness ratio, $E_m t_m/E_c t_c$, such that

$$\frac{E_m t_m}{E_c t_c} > \left(\frac{E_m t_m}{E_c t_c}\right)_{crit} \tag{11}$$

leads to multiple cracking. The critical layer stiffness ratio, $(E_m t_m/E_c t_c)_{crit}$, depends only on the nondimensional pre-crack length, $a_0/(t_m + t_c)$,

$$\left(\frac{E_m t_m}{E_c t_c}\right)_{crit} = f_{ELAS}\left(\frac{a_0}{t_m + t_c}\right). \tag{12}$$

The nondimensional function, f_{ELAS}, is shown in Fig. 3, along with the LEFM result, d_{LEFM} in eqn (6), for identical metal–ceramic moduli. [There is a rather weak dependence on the Poisson's ratios of metal and ceramic in eqn (12). The differences in σ_{max} for various Poisson's ratios are less than 0.3%, so the Poisson's ratios are fixed as $\nu_c = 0.3$ and $\nu_m = 0.33$.] The curve separates the damage mode in a metal–ceramic laminate predicted by the present elastic model: multiple cracking dominates above the curve and single-crack extension prevails below the curve.

Contrary to the LEFM results, the elastic model clearly shows a dependence of the critical stiffness ratio on the pre-crack length. Moreover, the critical thickness ratio, $(t_m/t_c)_{crit}$, estimated by the elastic model for $E_m = E_c$ is significantly larger than that by the LEFM model. Although the discrepancies between the LEFM and elastic models in the prediction of multiple cracking need to be compared with experimental data in order to check the validity, the following conclusion from the elastic model always holds: the critical metal–ceramic layer thickness ratio, $(t_m/t_c)_{crit}$, must increase if the metal–ceramic moduli ratio, E_m/E_c, decreases.

4.2. *Dugdale model*

Metal plasticity plays an important role in the damage mode competition between multiple cracking and single-crack extension. It reduces the stress concentrations near tips of the pre-crack and renucleated crack, thus the load carried by the metal layer between two cracks [layer m_1 in Fig. 1(a)] is shed to adjacent layers. This will increase the probability of single-crack extension being the damage mode.

A simple plasticity model in fracture mechanics, the Dugdale model, is applied to the shear-lag analysis to examine the effect of metal plasticity, in particular, yield stress. For the first two unbroken metal layers [m_1 and m_2 in Fig. 1(a)] i.e. the metal layer between two cracks and the one next to the renucleated crack, the maximum stress in each metal layer occurs at the crack plane (i.e. plane $y = 0$) due to the stress concentration near the pre-crack and renucleated crack. This has also been verified by the elastic model in the previous section. As the remote loading increases, the first unbroken metal layer (i.e. the one between two cracks) yields first at $y = 0$, when the stress at $y = 0$ in the layer reaches a critical value $\bar{\sigma}_Y$ and $\bar{\sigma}_Y = \rho\sigma_Y$, where σ_Y is the uniaxial tensile yield stress of the metal and the nondimensional parameter ρ characterizes the constraint from the adjacent layers in the laminate and reflects the stress triaxiality. For example, Ashby *et al.* (1989) established that the constraint parameter ρ can be as high as five in constrained metal wires, which was also verified by Huang *et al.* (1991) and Tvergaard *et al.* (1992). Two estimates for the constraint parameter ρ for metal–ceramic laminates based on different approaches are given in the Appendix. The first estimate is based on elastic fracture mechanics for laminates and ρ is given by

$$\rho = \frac{1}{1 - 2\nu_m}, \tag{13}$$

where ν_m is the Poisson's ratio of the metal. For a typical value, $\nu_m = 0.33$, ρ is 2.94, hence the bridging stress in the metal layer between two cracks [layer m_1 in Fig. 1(a)] is almost three times the yield stress. The second estimate for ρ is based on Prandtl's solution for

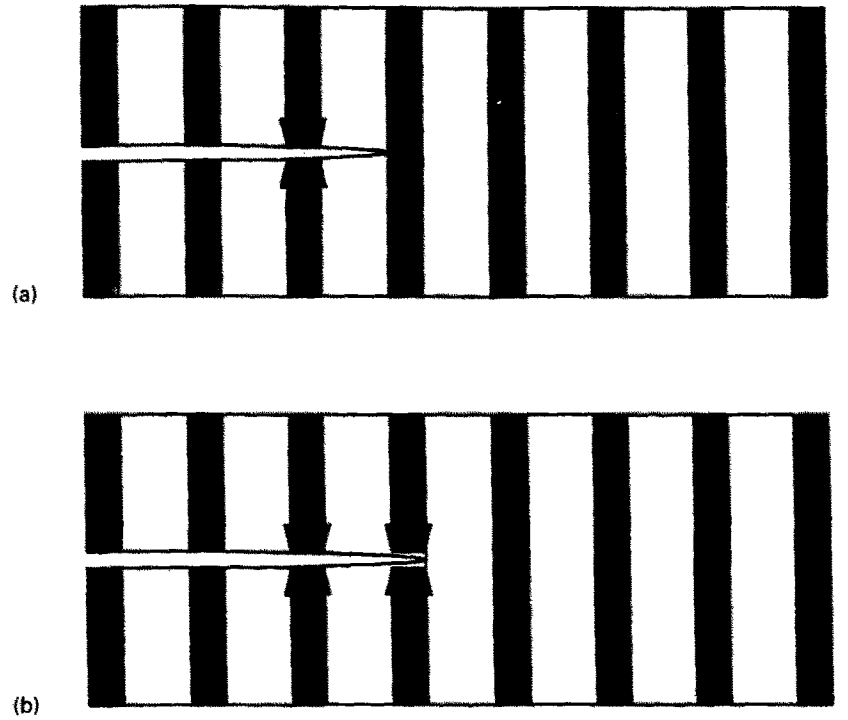

Fig. 6. Dugdale shear-lag model: (a) plastic yielding in the first unbroken metal layer; (b) plastic yielding in the first and second unbroken metal layers.

plastic stress fields for a perfectly plastic solid containing one crack or two coplanar cracks. The corresponding ρ is given by

$$\rho = \frac{2+\pi}{\sqrt{3}} = 2.97, \tag{14}$$

which agrees very well with the first estimate in eqn (13) for metals. It should be emphasized that the constraint parameter ρ can be higher than three for a well-bonded metal–ceramic interface and lower than three for a poorly bonded interface (Ashby *et al.*, 1989).

For further increases in the applied stress, the stress at $y = 0$ in the metal layer between two cracks [layer m_1 in Fig. 1(a)] is assumed to stay at $\bar{\sigma}_Y$ and the plastic flow is limited to the plane $y = 0$ in the metal layer in such a fashion that the metal layer on two sides of the crack plane starts to "separate" [Fig. 6(a)], as in the Dugdale model. Following the "separation," the maximum stress (i.e. stress at $y = 0$) in the next metal layer [layer m_2 in Fig. 1(a)] will continue to increase and reach $\bar{\sigma}_Y$ ($= \rho\sigma_Y$) eventually with the increase in applied load. As shown in Fig. 6(b), the metal layer next to the renucleated crack [layer m_2 in Fig. 1(a)] also becomes "separated" at plane $y = 0$, where the stress in the layer is fixed at $\bar{\sigma}_Y$. [It must be emphasized that the maximum stress in the third unbroken metal layer, i.e. layer m_3 in Fig. 1(a), does not necessarily occur at the crack plane $y = 0$. Therefore, the Dugdale model cannot be extended to $y = 0$ in the third unbroken metal layer.]

It is evident that the Dugdale model has not captured the effect of strain hardening in metal because metal plasticity is limited to the crack plane. Moreover, even for an elastic–perfectly plastic metal, the present model overestimates the probability of single-crack extension due to "separation" in this model. Though large plastic deformation in metal layers near two cracks has been observed (Shaw *et al.*, 1993), the metal layers remain intact such that the actual deformation around the crack plane in metal layers is less than that estimated by the Dugdale model. Thus, the stress at $y = 0$ in the first unbroken ceramic layer [layer c_2 in Fig. 1(a)], i.e. σ_0 given in eqn (5), is overestimated. {There is another limit to the level of applied stress in the Dugdale model because the maximum stress in the third

unbroken metal layer [layer m_3 in Fig. 1(a)], which may not occur at $y = 0$, must be less than $\bar{\sigma}_Y$.}

The applied stress plays a role in the competition between multiple cracking and single-crack extension due to metal plasticity. Let ε^∞ denote the remote strain, which is related to applied stress by eqn (8). The plane-strain yield strain of the metal is related to uniaxial tensile yield stress, σ_Y, by

$$\bar{\varepsilon}_Y = \frac{(1-\nu_m^2)\sigma_Y}{\sqrt{1-\nu_m+\nu_m^2}\,E_m} = \frac{\bar{\sigma}_Y}{\rho\sqrt{1-\nu_m+\nu_m^2}\,\bar{E}_m}, \tag{15}$$

where $\bar{E}_m = E_m/(1-\nu_m^2)$ is the plane-strain tensile modulus. The ratio of $\varepsilon^\infty/\bar{\varepsilon}_Y$ must be less than one to ensure that the remote field is elastic.

The governing equation is the same as the linear ordinary differential equation for the elastic model. The boundary conditions are also the same as in eqns (7) and (8) except for the first two unbroken metal layers, m_1 and m_2 in Fig. 1(a) (i.e. layers between two cracks and next to the renucleated crack). The boundary conditions at $y = 0$ in these two layers are

$$\sigma(y=0) = \bar{\sigma}_Y = \rho\sigma_Y \tag{16a}$$

or

$$w(y=0) = 0 \quad \text{if } \sigma(y=0) < \bar{\sigma}_Y = \rho\sigma_Y. \tag{16b}$$

It is noted that Fig. 6(a) applies at relatively small remote loading and Fig. 6(b) comes into play as remote loading increases.

The criterion for multiple cracking is the same as that in Sections 3 and 4.1: multiple cracking dominates if $\sigma_{max} > \sigma_0$, where σ_{max} is the maximum stress in the ceramic layer containing the renucleated crack and σ_0 is the stress at $y = 0$ in the next (unbroken) ceramic layer. The condition separating multiple cracking from single-crack extension is then $\sigma_{max} = \sigma_0$. These stresses have the form

$$\sigma_{max} = \sigma^\infty \Sigma_{max}^{III}\left(\frac{t_m}{t_c}, \frac{a_0}{t_m+t_c}, \frac{E_m}{E_c}\right) + \rho\sigma_Y \Sigma_{max}^{IV}\left(\frac{t_m}{t_c}, \frac{a_0}{t_m+t_c}, \frac{E_m}{E_c}\right) \tag{17}$$

$$\sigma_0 = \sigma^\infty \Sigma_0^{III}\left(\frac{t_m}{t_c}, \frac{a_0}{t_m+t_c}, \frac{E_m}{E_c}\right) + \rho\sigma_Y \Sigma_0^{IV}\left(\frac{t_m}{t_c}, \frac{a_0}{t_m+t_c}, \frac{E_m}{E_c}\right), \tag{18}$$

where Σs are nondimensional functions.

It is observed that, for all levels of applied stress and metal yield stress, σ^∞/σ_Y (or $\varepsilon^\infty/\bar{\varepsilon}_Y$), the conclusions established in the elastic model hold: for each metal–ceramic moduli ratio, there exists a critical thickness ratio of metal–ceramic layers above which multiple cracking dominates. Moreover, this critical thickness ratio is inversely proportional to the metal–ceramic moduli ratio such that eqn (11) still holds, i.e. the competition between multiple cracking and single-crack extension is governed by the metal–ceramic layer stiffness ratio. However, $(E_m t_m/E_c t_c)_{crit}$ now depends on not only the pre-crack length, $a_0/(t_m+t_c)$, but also on the applied stress level, $\varepsilon^\infty/\bar{\varepsilon}_Y$, and the constraint parameter ρ through the combination $\varepsilon^\infty/(\rho\bar{\varepsilon}_Y)$, i.e.

$$\left(\frac{E_m t_m}{E_c t_c}\right)_{crit} = f_{DUGD}\left(\frac{a_0}{t_m+t_c}, \frac{\varepsilon^\infty}{\rho\bar{\varepsilon}_Y}\right), \tag{19}$$

where f_{DUGD} is a nondimensional function. It is identical to the elastic model at small applied load (i.e. no plastic yielding),

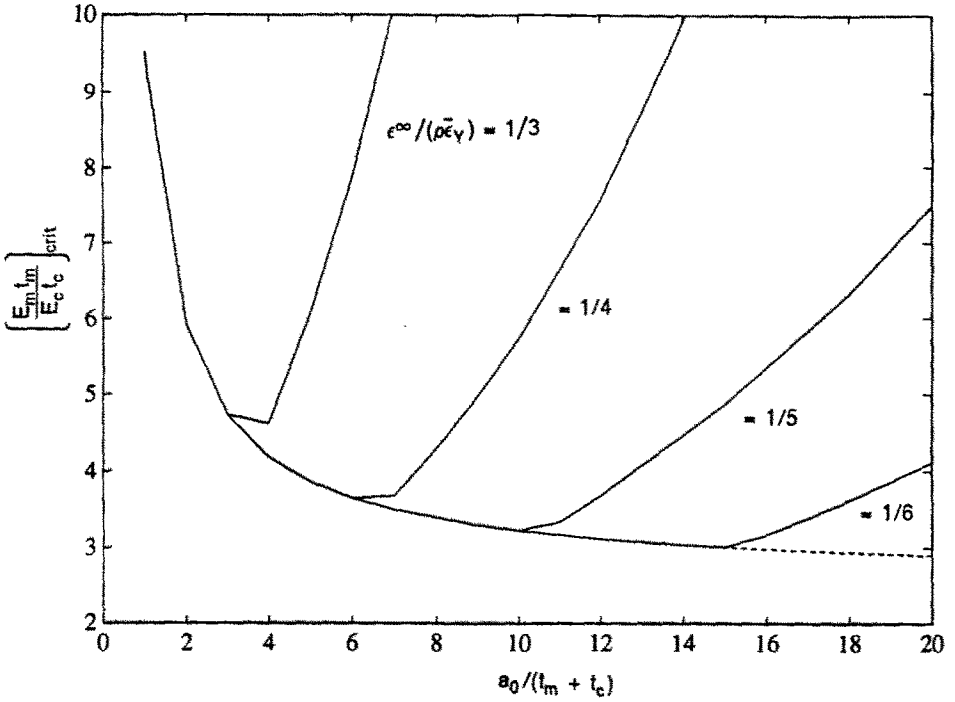

Fig. 7. Critical metal–ceramic layer stiffness ratio, $(E_m t_m/E_c t_c)_{crit}$, versus the pre-crack length, $a_0/(t_m+t_c)$, for $\varepsilon^\infty/(\rho\bar{\varepsilon}_Y) = 1/6$, 1/5, 1/4 and 1/3 in the Dugdale model.

$$f_{DUGD}\left(\frac{a_0}{t_m+t_c}, 0\right) = f_{ELAS}\left(\frac{a_0}{t_m+t_c}\right). \tag{20}$$

The critical layer stiffness ratio, $(E_m t_m/E_c t_c)_{crit}$, versus the pre-crack length, $a_0/(t_m+t_c)$, is shown in Fig. 7 for applied strain levels $\varepsilon^\infty/(\rho\bar{\varepsilon}_Y) = 1/6$, 1/5, 1/4 and 1/3. At each level of applied stress [i.e. $\varepsilon^\infty/(\rho\bar{\varepsilon}_Y)$], σ_{max} is larger than σ_0 above the corresponding curve, so multiple cracking may occur. For small pre-cracks, all curves are coincidental with the elastic results from Section 4.1 because the stress in metal layers does not reach $\bar{\sigma}_Y$ $(= \rho\sigma_Y)$ for small cracks and there is no plastic yielding in metal layers. The critical layer stiffness ratio, $(E_m t_m/E_c t_c)_{crit}$, deviates from that of the elastic model as the pre-crack length increases for a fixed $\varepsilon^\infty/(\rho\bar{\varepsilon}_Y)$. Moreover, the critical layer stiffness ratio increases for long pre-cracks, as opposed to a monotonic decreasing curve from the elastic model. The region governed by multiple cracking shrinks when plastic yielding occurs in metal layers. Therefore, plastic yielding in metals does not help in activating the multiple-cracking mode.

4.3. *Plastic model*

The Dugdale model in the previous section did not accurately account for the effect of plastic yielding in metal layers because the plastic deformation was assumed to be limited to a single plane. The model also neglected the plastic hardening of metals. These effects are studied in this section.

The metal is assumed to have an elastic–linear hardening stress–strain relation in uniaxial tension:

$$\begin{aligned} \sigma &= E_m\varepsilon, && \varepsilon \leqslant \frac{\sigma_Y}{E_m} \\ &= E_t\varepsilon + \left(1-\frac{E_t}{E_m}\right)\sigma_Y, && \varepsilon > \frac{\sigma_Y}{E_m} \end{aligned} \tag{21}$$

where σ_Y is the tensile yield stress, and E_m and E_t are elastic and linear hardening moduli,

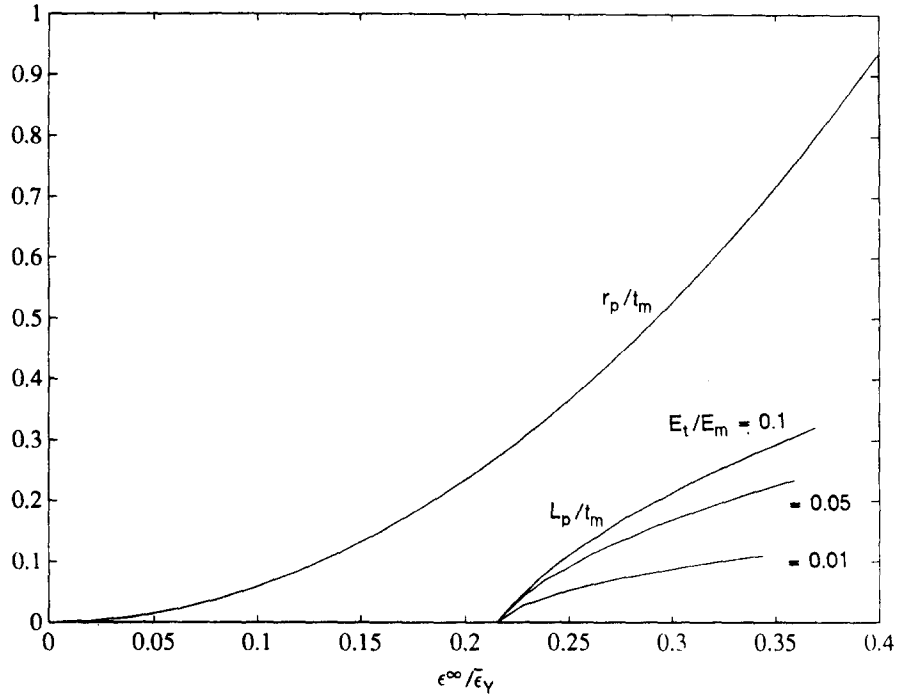

Fig. 8. Plastic zone size in the plastic model (L_p/t_m) and in small-scale-yielding in the LEFM model (r_p/t_m) versus $\varepsilon^\infty/\bar{\varepsilon}_Y$ for $E_m = E_c$, $t_m = t_c$, $a_0 = 5(t_m + t_c)$, and three plastic hardening levels, $E_t/E_m = 0.01$, 0.05 and 0.1.

respectively. The shear-lag analysis leads to a set of *nonlinear* ordinary differential equations (see the Appendix for details), and the boundary conditions remain the same as in eqn (7). The remote field is elastic (i.e. $\varepsilon^\infty < \bar{\varepsilon}_Y$), so eqn (8) holds.

Plastic zones grow in metal layers as the applied stress increases. The plastic zone's size, L_p, in the metal layer between two cracks [layer m_1 in Fig. 1(a)] versus the applied strain, $\varepsilon^\infty/\bar{\varepsilon}_Y$, is shown in Fig. 8 for $E_m/E_c = 1$; $t_m/t_c = 1$; and $a_0/(t_m + t_c) = 5$ and several values of the plastic hardening modulus, $E_t/E_m = 0.01$, 0.05 and 0.1. The plastic zone's size based on a small-scale-yielding estimation in the LEFM model (Kannien and Popelar, 1985),

$$r_p = \frac{1}{3\pi}\left(\frac{K_{tip}}{\sigma_Y}\right)^2, \tag{22}$$

is also shown in Fig. 8, where K_{tip} is the pre-crack tip stress intensity factor. These two models show reasonable agreement.

The criterion governing the damage mode as multiple cracking or single-crack extension is the same as in previous sections, $\sigma_{max} = \sigma_0$. They have the form

$$\sigma_{max} = \sigma^\infty \Sigma^V_{max}\left(\frac{t_m}{t_c}, \frac{a_0}{t_m + t_c}, \frac{E_m}{E_c}, \frac{E_t}{E_m}, \frac{\sigma_Y}{E_m}, \frac{\sigma^\infty}{\rho\sigma_Y}\right) \tag{23}$$

$$\sigma_0 = \sigma^\infty \Sigma^V_0\left(\frac{t_m}{t_c}, \frac{a_0}{t_m + t_c}, \frac{E_m}{E_c}, \frac{E_t}{E_m}, \frac{\sigma_Y}{E_m}, \frac{\sigma^\infty}{\rho\sigma_Y}\right), \tag{24}$$

where the last three arguments in the nondimensional functions Σ^V_{max} and Σ^V_0 represent the plastic hardening and yielding of metal and the applied stress level. Though Σ^V_{max} and Σ^V_0 depend on many parameters, the numerical solution of $\sigma_{max} = \sigma_0$ to determine the critical condition for multiple cracking shows that eqn (11) always holds, i.e. the competition of

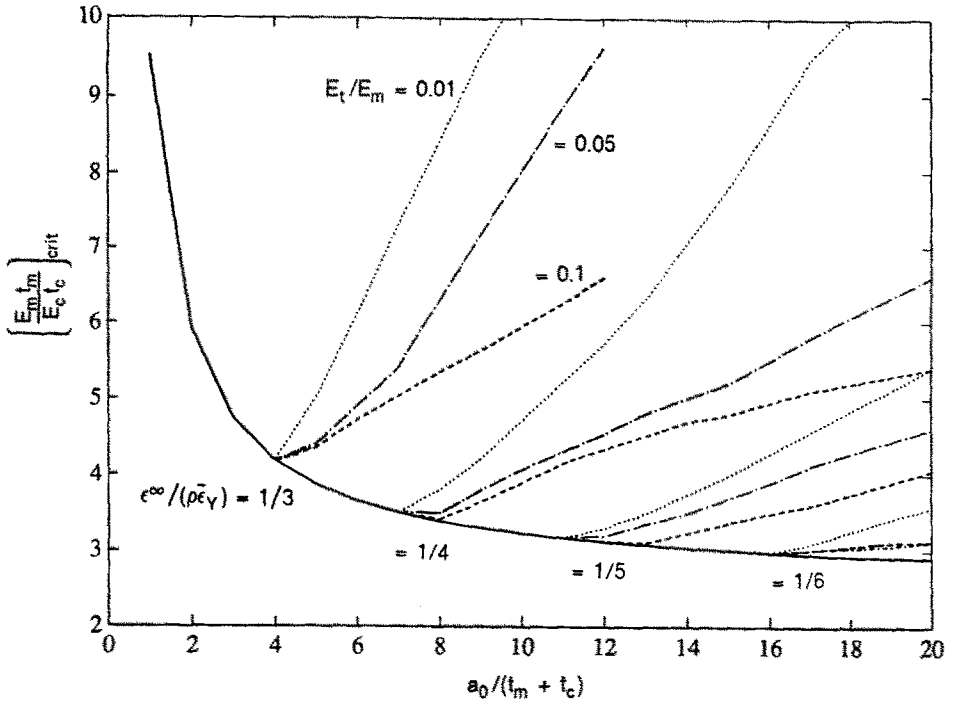

Fig. 9. Critical metal–ceramic layer stiffness ratio, $(E_m t_m/E_c t_c)_{crit}$, versus pre-crack length, $a_0/(t_m+t_c)$, for $\varepsilon^\infty/(\rho\bar{\varepsilon}_Y) = 1/6$, 1/5, 1/4 and 1/3; $\sigma_Y/E_m = 0.003$; and three plastic hardening levels, $E_t/E_m = 0.01$ (dotted lines), 0.05 (dashed–dotted lines and 0.1 (dashed lines) in the plastic model.

the multiple-cracking and single-crack extension damage modes is governed by the metal–ceramic layer stiffness ratio. The critical layer stiffness ratio has the form

$$\left(\frac{E_m t_m}{E_c t_c}\right)_{crit} = f_{PLAS}\left(\frac{a_0}{t_m+t_c}, \frac{E_t}{E_m}, \frac{\sigma_Y}{E_m}, \frac{\varepsilon^\infty}{\rho\bar{\varepsilon}_Y}\right). \tag{25}$$

It is identical to the elastic function, f_{ELAS}, if $E_t/E_m = 1$, or $\sigma_Y/E_m = \infty$, or $\varepsilon^\infty/(\rho\bar{\varepsilon}_Y) = 0$. The critical layer stiffness ratios, $(E_m t_m/E_c t_c)_{crit}$, versus pre-crack length, $a_0/(t_m+t_c)$, are shown in Fig. 9 for $\sigma_Y/E_m = 0.003$; several applied strain levels, $\varepsilon^\infty/(\rho\bar{\varepsilon}_Y) = 1/6$, 1/5, 1/4 and 1/3; and several plastic hardening levels, $E_t/E_m = 0.01$, 0.05 and 0.1. For each applied strain, $\varepsilon^\infty/(\rho\bar{\varepsilon}_Y)$, curves for various hardening moduli start to deviate from the elastic curve at the same point, corresponding to plastic yielding in the metal layer. These curves exhibit a trend similar to that in Fig. 7 for the Dugdale model, i.e. all curves coincide at small pre-crack lengths and the region controlled by multiple cracking shrinks as the applied stress increases. However, a comparison of Fig. 9 with Fig. 7 shows that the work hardening of metals can significantly enlarge the multiple-cracking domain. The probability of activating multiple cracking as the damage mode is increased greatly for a metal with strong plastic hardening (e.g. large tangent modulus E_t). The curves in Fig. 9 for weak work hardening ($E_t/E_m = 0.01$) are very close to the Dugdale model results (Fig. 7), which means the Dugdale model is a good model for an elastic–perfectly plastic solid. Based on these observations, one can conclude that plastic hardening helps activate the multiple-cracking mode, while plastic yielding does the opposite.

Acknowledgements—The first author (YH) greatly appreciates the suggestions and comments made by Professor Bernard Budiansky. Discussion with Professor A. G. Evans is also gratefully acknowledged.

REFERENCES

Ashby, M. F., Blunt, F. J. and Bannister, M. (1989). Flow characteristics of highly constrained metal wires. *Acta Metall.* **37**, 1847–1857.

Budiansky, B., Hutchinson, J. W. and Evans, A. G. (1986). Matrix fracture in fiber reinforced ceramics. *J. Mech. Phys. Solids* **34,** 167–189.
Cao, H. C. and Evans, A. G. (1991). On crack extension in ductile/brittle laminates. *Acta Metall.* **39,** 2997–3005.
Dalgleish, B. J., Lu, M. C. and Evans, A. G. (1988). The strength of ceramics bonded with metals. *Acta Metall.* **36,** 2029–2036.
Dalgleish, B. J., Trumble, K. P. and Evans, A. G. (1989). The strength and fracture of alumina bonded with aluminum alloys. *Acta Metall.* **37,** 1923–1931.
Deve, H. E., Evans, A. G. and Shih, D. (1992). A high-toughness gamma-titanium aluminide. *Acta Metall.* **40,** 1259–1265.
Deve, H. E. and Maloney, M. J. (1991). On the toughening of intermetallics with ductile fibers: the role of interfaces. *Acta Metall.* **39,** 2275–2284.
Erdogan, F., Gupta, G. D. and Cook, T. S. (1973). Numerical solution of singular integral equations. In *Methods of Analysis and Solutions of Crack Problems* (Edited by G. C. Sih), pp. 386–425. Noordhoff, Leyden, The Netherlands.
Evans, A. G., Lu, M. C., Schmauder, S. and Ruhle, M. (1986). Some aspects of the mechanical strength of ceramic/metal bonded systems. *Acta Metall.* **34,** 1643–1655.
Hill, R. (1950). *The Mathematical Theory of Plasticity*. Oxford University Press, Oxford.
Huang, Y., Hutchinson, J. W. and Tvergaard, V. (1991). Cavitation instabilities in elastic–plastic solids. *J. Mech. Phys. Solids* **39,** 223–241.
Kannien, M. F. and Popelar, C. H. (1985). *Advanced Fracture Mechanics*. Oxford University Press, New York.
Kuhn, P. (1956). *Stresses in Aircraft and Shell Structures*. McGraw-Hill, New York.
Rice, J. R. (1968). Mathematical analysis in the mechanics of fracture. In *Fracture—An Advanced Treatise*, Vol. II (Edited by H. Liebowitz), pp. 191–308. Academic Press, New York.
Rubinstein, A. A. (1985). Macrocrack interaction with semi-infinite microcrack array. *Int. J. Fracture* **27,** 113–119.
Shaw, M. C., Marshall, D. B., Dadkhah, M. S. and Evans, A. G. (1993). Cracking and damage in ceramic/metal multilayers. *Acta Metall.* **41,** 3311–3322.
Suo, Z. (1989). Singularities interacting with interfaces and cracks. *Int. J. Solids Structures* **25,** 1133–1142.
Tvergaard, V., Huang, Y. and Hutchinson, J. W. (1992). Cavitation instabilities in a power hardening elastic–plastic solid. *Eur. J. Mech., A/Solids* **11,** 215–231.

APPENDIX

Integral equations for metals and ceramics with identical elastic properties

The metal–ceramic laminate can be considered as a uniform medium if the metal and ceramic have the same elastic properties. Then, each crack can be modeled as a continuous distribution, with the dislocation densities to be determined (Rice, 1968). The laminate is traction-free on the left boundary and subject to remote axial stress, σ^{∞} [Fig. 1(a)]. The stress field induced by an edge dislocation at $(\xi, 0)$ in a half-plane (traction-free on the boundary of the half-plane) can be found in Suo (1989). In particular, the stress component in the laminate direction at a point $(x, 0)$ is

$$K(x,\xi)=\sigma_{yy}|_{y=0}=\frac{\bar{E}_m}{4\pi}\left[\frac{1}{\xi-x}+\frac{(x+a_0)^2-(\xi+a_0)^2+4(\xi+a_0)(x+\xi_0)}{(\xi+x+2a_0)^3}\right], \tag{A1}$$

where a_0 is the pre-crack length and the origin (0, 0) is set at the pre-crack tip, as shown in Fig. 1(a). Then, the traction-free condition at the surfaces of pre-crack and renucleated cracks leads to

$$\sigma^{\infty}+\int_{-a_0}^{0}K(x,\xi)\frac{\mathrm{d}\delta^{(1)}}{\mathrm{d}\xi}\mathrm{d}\xi+\int_{t_m}^{t_m+t_c}K(x,\xi)\frac{\mathrm{d}\delta^{(2)}}{\mathrm{d}\xi}\mathrm{d}\xi=0 \tag{A2}$$

$$\text{for } -a_0<x<0 \text{ (pre-crack)}$$

$$t_m<x<t_m+t_c \text{ (renucleated crack)}$$

where $\delta^{(1)}$ and $\delta^{(2)}$ are the crack opening at the pre-crack and renucleated crack, respectively. These integral equations of $\delta^{(1)}$ and $\delta^{(2)}$ are solved numerically along the lines proposed by Erdogan *et al.* (1973).

Shear-lag analysis of metal–ceramic laminates

The shear-lag analysis was initially developed for single or multiple stringer panels in aerospace structures (e.g. Kuhn, 1956). It has been successfully applied to metal–ceramic laminates (e.g. Cao and Evans, 1991). Each layer in the laminate is subject to remote applied loading and shear tractions at the interfaces with neighboring layers [Fig. 1(a)]. Let n be the layer number, and a metal layer and a ceramic layer correspond to an odd and even number of n, respectively. For example, layer 1 is the leftmost metal layer of the laminate.

The axial stress in each layer is averaged over the layer thickness and is then independent of coordinate x. At each cross section (i.e. each y) in a layer, overall equilibrium requires

$$t_n\frac{\mathrm{d}\sigma_n}{\mathrm{d}y}=\tau_n^{\mathrm{L}}+\tau_n^{\mathrm{R}}, \tag{A3}$$

where t_n is the thickness of the layer, i.e. $t_n=t_m$ if n is odd and $t_n=t_c$ if n is even; τ_n^{L} and τ_n^{R} are shear tractions (downward) at the left and right boundaries of the nth layer, and $\tau_1^{\mathrm{L}}=0$ due to traction-free conditions at the leftmost boundary of the laminate [Fig. 1(a)]. Let $w_n(y)$ be the axial displacement at the center of the cross section

and w_n^L and w_n^R be the axial displacement at the interfaces between layer n and its two neighboring layers ($n-1$ and $n+1$, respectively). The shear tractions are related to shear strains and displacements by

$$\tau_n^L = G_n\gamma_n^L = G_n\frac{w_n - w_n^L}{t_n/2}, \quad \tau_n^R = G_n\gamma_n^R = G_n\frac{w_n - w_n^R}{t_n/2}, \tag{A4}$$

where G_n is the shear modulus in the layer, $G_n = G_m$ if n is odd, and $G_n = G_c$ if n is even.

The continuity of displacements and shear tractions at metal–ceramic interfaces requires

$$w_n^L = w_{n-1}^R, \quad w_n^R = w_{n+1}^L \tag{A5}$$

$$\tau_n^L = -\tau_{n-1}^R, \quad \tau_n^R = -\tau_{n+1}^L \tag{A6}$$

(since the τs are assumed downward!). Equations (A4–A6) can be rearranged to eliminate the displacements at interfaces,

$$\tau_n^L = 2\frac{w_n - w_{n-1}}{\dfrac{t_m}{G_m} + \dfrac{t_c}{G_c}}, \quad \tau_n^R = 2\frac{w_n - w_{n+1}}{\dfrac{t_m}{G_m} + \dfrac{t_c}{G_c}}. \tag{A7}$$

The substitution of eqn (A7) into eqn (A3) eliminates shear tractions,

$$t_n\frac{d\sigma_n}{dy} = 2\frac{2w_n - w_{n-1} - w_{n+1}}{\dfrac{t_m}{G_m} + \dfrac{t_c}{G_c}}. \tag{A8}$$

The elastic stress–strain relation in the nth layer is

$$\sigma_n = \bar{E}_n\frac{dw_n}{dy}, \tag{A9}$$

where $\bar{E}_n$ is the plane-strain tensile modulus, i.e. $\bar{E}_n = \bar{E}_m$ if n is odd and $\bar{E}_n = \bar{E}_c$ if n is even. Equations (A8) and (A9) form a set of linear ordinary differential equations governing σ_n and w_n. For plastic deformation in metal layers, the stress–strain relation is

$$\begin{aligned}
\sigma_n &= \bar{E}_c\frac{dw_n}{dy} && n \text{ even} \\
&= \bar{E}_m\frac{dw_n}{dy} && n \text{ odd and } \frac{dw_n}{dy} \leqslant \bar{\varepsilon}_Y \\
&= \bar{E}_t\frac{dw_n}{dy} + (\bar{E}_m - \bar{E}_t)\bar{\varepsilon}_Y && n \text{ odd and } \frac{dw_n}{dy} > \bar{\varepsilon}_Y
\end{aligned} \tag{A10}$$

where $\bar{E}_t$ is the plane-strain hardening modulus, and $\bar{\varepsilon}_Y$, as defined in eqn (15), is the plane-strain yield strain. The governing equations, (A8) and (A10), become a set of nonlinear ordinary equations.

Estimates of constraint parameter for a metal–ceramic laminate

Rubinstein (1985) studied the interaction between a macroscopic crack and a coplanar microcrack in a homogeneous solid. His closed-form solution shows that, within the ligament between two cracks, the stress component parallel to the cracks, σ_{xx}, is the same as the component normal to the crack direction, σ_{yy}. Thus, the stress state in the ligament between cracks is

$$\sigma_{xx} = \sigma_{yy}, \quad \sigma_{zz} = 2\nu\sigma_{yy}, \quad \text{others} = 0, \tag{A11}$$

where the out-of-plane stress component is obtained by the plane-strain condition $\varepsilon_{zz} = 0$. The numerical solution of the integral equation in eqn (A2) shows that the conclusion established in eqn (A11) approximately holds for the configuration in Fig. 1(a). Hence, the effective stress is

$$\sigma_e = \sqrt{\tfrac{1}{2}[(\sigma_{xx} - \sigma_{yy})^2 + (\sigma_{yy} - \sigma_{zz})^2 + (\sigma_{zz} - \sigma_{xx})^2]} = (1 - 2\nu)\sigma_{yy}. \tag{A12}$$

Recall that, in the Dugdale model, the effective stress ahead of the crack is set equal to the uniaxial yield stress, σ_Y, of the material. For *plane-stress* conditions ($\sigma_{zz} = 0$), it leads to $\sigma_{yy} = \sigma_Y$. For *plane-strain* conditions, as in the present study, eqn (A12) gives

$$\sigma_{yy} = \frac{\sigma_Y}{1 - 2\nu}, \tag{A13}$$

which leads to the constraint parameter ρ as given in eqn (13).

The estimate in eqn (A13) is based on elastic fracture mechanics. The estimate in the following includes the effect of metal plasticity. Prandtl's field (e.g. Hill, 1950) provides the stress state near a crack tip or between two

cracks in an elastic–perfectly plastic solid. In particular, the stress component normal to the crack direction within the ligament between two cracks is

$$\sigma_{yy} = (2+\pi)\tau_Y = (2+\pi)\frac{\sigma_Y}{\sqrt{3}}, \tag{A14}$$

where $\tau_Y = \sigma_Y/\sqrt{3}$ is the yield stress in pure shear. Hence, the estimate of ρ in eqn (14) is obtained. For a typical value of Poisson's ratio, $\nu = 0.33$, the two estimates in eqns (13) and (14), or in eqns (A13) and (A14), agree very well.